Investigation of a Fluorine-Free Phosphonium-Based Ionic Liquid Electrolyte and Its Compatibility with Lithium Metal

Niyousha Karimi, Maider Zarrabeitia, Milad Hosseini, Tugce Ates, Boyan Iliev, Thomas J. S. Schubert, Alberto Varzi,* and Stefano Passerini*

ABSTRACT: A novel fluorine-free ionic liquid electrolyte comprising lithium dicyanamide (LiDCA) and trimethyl(isobutyl)-phosphonium tricyanomethanide (P_{111i4}TCM) in a 1:9 molar ratio is studied as an electrolyte for lithium metal batteries. At room temperature, it demonstrates high ionic conductivity and viscosity of about 4.5 mS cm^{-1} and 64.9 mPa s, respectively, as well as a 4 V electrochemical stability window (ESW). Li stripping/plating tests prove the excellent electrolyte compatibility with Li metal, evidenced by the remarkable cycling stability over 800 cycles. The evolution of the Li−electrolyte interface upon cycling was investigated via electrochemical impedance spectroscopy, displaying a relatively low impedance increase after the initial formation cycles. Finally, the solid electrolyte interphase (SEI) formed on Li metal appeared to have a bilayer structure mostly consisting of DCA and TCM reduction products. Additionally, decomposition products of the phosphonium cation were also detected, despite prior studies reporting its stability against Li metal.

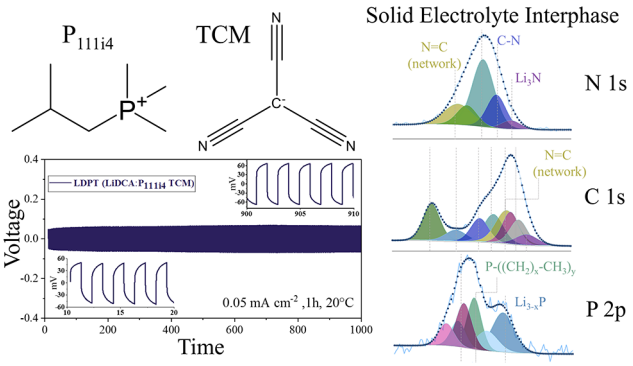

KEYWORDS: *Li metal anode, lithium metal battery, fluorine-free ionic liquid electrolyte, phosphonium cation, solid electrolyte interphase*

INTRODUCTION

A promising path to enhance the performance of lithium-based batteries, especially in terms of energy density, is the employment of safe and durable Li metal electrodes.[1,2] In fact, despite providing a large specific capacity (3861 mAh g^{-1}) and a very negative potential (−3.05 V vs SHE), Li metal anodes suffer from safety hazards and short life cycle, limiting the commercialization of rechargeable Li-metal batteries.[1]

Li metal, however, also shows high reactivity toward most electrolytes. This leads to the spontaneous formation of a solid electrolyte interphase (SEI) at the electrode/electrolyte interface.[3] The properties of such SEI are crucial to enable reversible plating and stripping. In fact, upon charging of the cell, the Li metal surface is regenerated, and, in the absence of a stable SEI, continuous electrolyte decomposition could take place, resulting in capacity loss. The safety issues are mostly associated with the formation of Li dendrites due to a nonuniform deposition of Li.[4] The dendritic deposits can potentially grow through the separator, resulting in a short-circuit. Such phenomena create significant local heating and introduce the risk of fire or explosion when organic electrolytes based on highly volatile and flammable solvents are used.[5] In addition, the commonly used conducting salt, lithium hexafluorophosphate ($LiPF_6$), also suffers from low thermal stability and high sensitivity to water.[6,7] Hydrofluoric acid (HF), which is easily formed by a $LiPF_6$ reaction with even a trace amount of moisture, is toxic, corrosive, and can have a detrimental impact on the battery performance.[8,9]

Among the possible solutions for circumventing these problems is the replacement of conventional carbonate-based electrolytes with safer ionic liquid (IL)-based electrolytes.[10] ILs are molten salts at room temperatures, offering a unique set of properties such as negligible flammability and volatility, high thermal stability, and a wide ESW, all of which can enhance the safety of LIBs.[11−13]

Moving toward safer and more environmentally friendly electrolytes,[14−19] we have specifically focused on a fluorine-free class of ILs based on dicyanamide (DCA) and tricyanomethanide (TCM) anions, which have shown promising results as an electrolyte for Li-metal electrodes.[20,21] These cyano-based ILs exhibit very low viscosity and significantly high ionic conductivity owing to their small anion size,[22] good charge delocalization, and great symmetry in the case of TCM

anions.[23] Additionally, the lower density of these ILs compared to the state-of-the-art bis(trifluoromethanesulfonyl)imide (TFSI)- and bis(fluoromethanesulfonyl)imide (FSI)-based ILs can potentially lead to higher specific energy density, as well as increased safety and lower production costs due to the absence of fluorine.[21,22,24,25]

Among the large variety of available ILs, the most investigated ones for lithium-ion battery (LIB) applications are those based on quaternary ammonium, pyrrolidinium, and imidazolium cations.[12,21,26−32] Nevertheless, in recent years, ILs containing the phosphonium cation were successfully introduced as well.[33−35] In particular, recent studies on phosphonium cations with small alkyl chains, trimethyl-(isobutyl)phosphonium (P_{111i4}), combined with the FSI anion, have shown remarkable stability with Li metal.[34,36,37] The outstanding cycling efficiency and cycling performance of the electrolyte on the Li metal were attributed to the formation of a stable SEI at the Li metal electrode.[38] The formed SEI exhibited a layered structure with significant quantities of chemical species associated with the FSI anion reduction, such as lithium fluoride (LiF), lithium oxide (Li_2O), and lithium sulfide (Li_2S, $LiSO_2$, and Li_2NSO_2F), whereas no evidence of P_{111i4} cation reduction was found.[38]

Inspired by the potential of the P_{111i4} cation, in this study, we are presenting a novel electrolyte based on P_{111i4}TCM and LiDCA as a fluorine-free IL electrolyte for Li metal anode. The physicochemical and electrochemical properties of both the neat P_{111i4}TCM IL and the LiDCA-P_{111i4}TCM electrolyte (1:9 molar ratio) are studied with regard to ionic conductivity, viscosity, electrochemical stability, and, only for the latter, Li electrodeposition/dissolution behavior in Li/Li symmetrical cells. Additionally, the SEI formed during cycling on Li metal is characterized by X-ray photoelectron spectroscopy (XPS) and electrochemical impedance spectroscopy (EIS). This article represents the first report of a fluorine-free phosphonium IL electrolyte with Li metal.

EXPERIMENTAL SECTION

Electrolyte Preparation. The ionic liquid trimethyl(isobutyl)-phosphonium tricyanomethanide (P_{111i4}TCM, referred to as PT hereafter) and the Li salt, lithium dicyanamide (LiDCA) were provided by IoLiTec GmbH in a purity of >99.5%. Both IL and the Li salt were dried following the procedure previously reported.[20] The water content of the neat IL was measured using a Karl Fischer coulometric titration (Mettler Toledo Titrator Compact C30). The water content detected in all samples was <20 ppm (detection limit = 10 ppm). Both dry solutions were transferred directly into a glove box filled with Ar (LABmaster, MBRAUN GmbH, Germany, O_2 <0.1 ppm, H_2O <0.1 ppm), and they were stored and used for cell assembly. The LiDCA-P_{111i4}TCM electrolyte (1:9 mol/mol, corresponding to 0.49 mol kg $^{-1}$, referred to as LDPT hereafter) was prepared and stored inside the glove box. Figure 1 shows the structure of the complex ions present in the investigated electrolyte (LDPT).

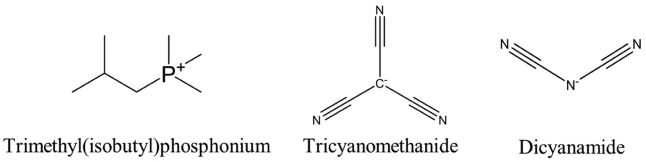

Trimethyl(isobutyl)phosphonium (P_{111i4}^+) | Tricyanomethanide (TCM^-) | Dicyanamide (DCA^-)

Figure 1. Chemical structure of the complex ions present in the electrolyte (LDPT).

Physicochemical Characterization. Ionic conductivity experiments were performed using an automatic conductivity meter (MCS 10, Bio-Logic) featuring a frequency analyzer and a climatic chamber, over temperatures ranging from 0 to 60 °C. At each temperature, a rest time of 2 h was allowed to reach equilibrium. Inside the glove box, PT and LDPT were included in sealed conductivity cells consisting of a glass housing and two platinized Pt electrodes. The cell constant was determined using a 0.01 mol/L KCl standard solution and was found to be 1.00 ± 0.01 cm $^{-1}$.

An Anton-Paar Physica MCR 301 rheometer was employed to measure viscosity. The tests were carried out in the 0−60 °C temperature range at 10 °C interval steps. The same shear rate of 50 s $^{-1}$ was used for all experiments.

Electrochemical Tests. Electrochemical investigations were carried out with three-electrode (Swagelok-type) cells. The cells were assembled in the same glove box used for sample preparation (see above). The ESW of PT and LDPT was investigated via linear sweep voltammetry (LSV). LSV experiments were performed using a Pt disk electrode (with 1 mm diameter) as a working electrode (WE) and a Li metal foil (500 μm thick, 99% battery grade, Honjo Metal, Japan) as both counter and reference electrodes (CE and RE). Prior to each experiment, the platinum electrode was polished.[39] LSV experiments were performed with a VMP-3 potentiostat/galvanostat (Bio-Logic Science Instruments, France) by scanning the WE potential starting from the open-circuit voltage (OCV) with a scan rate of 1 mV s $^{-1}$. One cell was assembled for either the anodic or the cathodic stability measurement, which was conducted at 20.0 ± 0.1 °C.

The Li^+ transference number was determined using two Li-metal disks as nonblocking electrodes in Li/LDPT/Li symmetric cells. After 2 h at the OCV, a constant voltage of 10 mV was applied, and the current decay was recorded for 10 h. The ratio between the stationary state current at the end of the potential step (I_{ss}) and the initial current at $t = 0$ (I_0) is the lithium transference number. Li stripping/plating experiments were also carried out in symmetrical Li/LDPT/Li cells with an applied current of 0.05 mA cm $^{-2}$ (1 h for each step). Electrochemical impedance spectra of such cells were collected at the OCV every 24 h of cycling in the frequency range between 1 MHz and 10 mHz using a 5 mV sinus amplitude.

Li/$LiFePO_4$ three-electrode half-cells were assembled using Li metal as the CE and RE and cathodes with an active material ($LiFePO_4$, LFP) loading of ca. 1 mg cm $^{-2}$. For details about the cathode composition and fabrication procedure, please refer to ref 67. The cells were galvanostatically cycled at C/10 (1C = 170 mA g $^{-1}$) at 20 °C in the voltage range of 2.8−4 V vs Li/Li^+.

X-ray Photoelectron Spectroscopy (XPS). For XPS measurements, the Li metal electrode was subjected to one deposition cycle for 1 h at 0.05 mA cm $^{-2}$ in Li symmetrical cell employing LDPT as the electrolyte. The details about sample preparation and XPS experimental setup are provided in ref 20. Due to the absence of a clear hydrocarbon peak in the C 1s spectrum commonly selected as a reference, the fitting of the spectra was performed without calibration but considering the binding energy separation of those species present in two or more photoelectron regions.[20,40,41]

RESULTS AND DISCUSSION

Physicochemical Characterization. The physicochemical and electrochemical characterization of PT and LDPT are shown in Figure 2. It should be noted that, prior to such experiments, the reactivity of both samples toward Li metal was visually evaluated by immersing a piece of Li foil in the PT and LDPT solutions (inside the glove box). Figure S1 shows photographs of the solutions in contact with Li metal after storage at room temperature (in a glove box) for different periods of time (i.e., just immersed, 10 min, 6 h, and 1 month). No color change can be observed, neither for the solutions nor for the Li metal that maintains its original metallic luster, suggesting its stability in contact with both IL-based solutions.

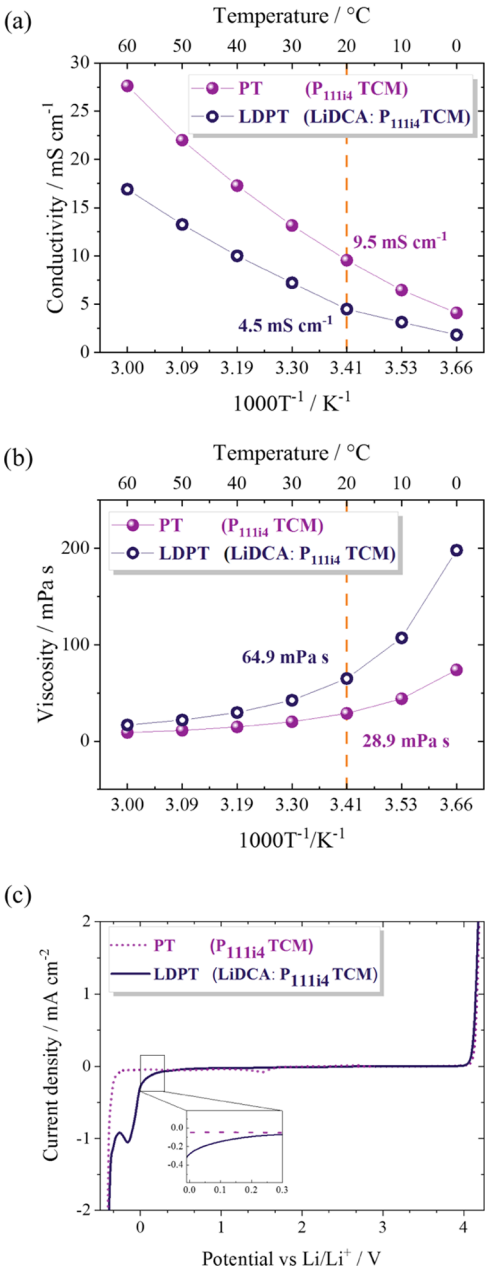

Figure 2. (a) Ionic conductivity and (b) viscosity vs temperature plots of PT and LDPT from 0 to 60 °C (heating rate of 5 °C h $^{-1}$). (c) Linear sweep voltammograms of Li/PT/Pt and Li/LDPT/Pt cells (both with Li as the RE) collected with a sweep rate of 1 mV s $^{-1}$ at 20 °C.

Variations in the ionic conductivity and viscosity with temperature are displayed in Figure 2a,b, respectively. With regard to PT, the ionic conductivity increased with increasing temperature, i.e., from 4.1 mS cm^{-1} at 0 °C to 9.5 mS cm^{-1} at 20 °C and, eventually, to 27.6 mS cm^{-1} at 60 °C. Following the inverse relation of ionic conductivity and viscosity, the latter (Figure 2b) decreased with temperature from 74 mPa s at 0 °C to 28.8 mPa s at 20 °C and 8.9 mPa s at 60 °C.

When the Li salt was added, a drop in conductivity and an increase in viscosity were observed for LDPT. As shown in Figure 2a,b at 20 °C, LDPT exhibited an ionic conductivity and viscosity of 4.5 mS cm^{-1} and 64.9 mPa s, respectively. Nevertheless, such behavior is expected considering the high surface charge density of Li^+ and, consequently, the strong Li^+-anion interactions. These strong interactions also increase the viscous drag, reducing the total ionic conductivity of the electrolyte compared to neat IL.[29]

Interestingly, the conductivity values of PT were higher than those reported for its fluorinated equivalent $P_{111i4}FSI$ (6.4 mS cm^{-1} and 41 mPa s at 20 °C)[34] and only slightly lower than those for the standard carbonate-based electrolyte ($LiPF_6$-EC-EMC 9.1 mS cm^{-1} at 25 °C).[42] Regarding LDPT, the ionic conductivity was also higher than that of a similar molal concentration FSI-based electrolyte with the same cation (0.5 mol kg^{-1} LiFSI-$P_{111i4}FSI$, i.e., 1:6.14 mol/mol, $\sigma \approx 3.5$ mS cm^{-1} at 20 °C)[34] and well above the 0.5 mol kg^{-1} LiTFSI-$Pyr_{14}TFSI$ (≈1.1 mS cm^{-1} at 20 °C),[27] rendering LiDCA-$P_{111i4}TCM$ an interesting electrolyte candidate for lithium metal batteries (LMBs).

In addition to ionic conductivity, the Li^+ transference number is a critical factor in determining the applicability of an electrolyte. The transference number of the LDPT electrolyte was determined to be 0.28, as calculated from the current decay reaching a steady-state upon 10 h of constant voltage applied to the cell (see Figure S2). Such a value is in line with the majority of liquid electrolytes.

Figure 2c illustrates the linear sweep voltammetries performed with PT and LDPT. Upon the anodic scan, the oxidation onset appeared at 4.1 V vs Li/Li^+. A similar anodic limit observed for both PT and LDPT is expected, considering the majority of the samples consist of TCM anions. This result is also in agreement with the recently reported value for the *N*-methyl-*N*-butylpyrrolidinium tricyanomethanide ($Pyr_{14}TCM$), evidencing the role of the anion in the anodic limit.[20] Upon reduction, the first small current peak appeared at 1.5 V vs Li/Li^+ for PT, followed by a severe increase in the cathodic current at −0.25 V vs Li/Li^+. In view of the major role that the reduction of the organic cation has with regard to the cathodic limit of the IL, this result evidences the higher stability of phosphonium compared to pyrrolidinium cations when paired with the same anion. In fact, $Pyr_{14}TCM$ exhibited cathodic decomposition starting from 1 V vs Li/Li^+.[20]

The addition of lithium salt is often expected to improve the cathodic stability of neat ILs.[30,43−48] In fact, the strong Coulombic interaction between the small Li^+ ions and the anion promotes the reduction of the anions to form a passivation layer on the electrode. This passivation layer would then prevent the severe reduction of the organic cation and extend the cathodic limit.[48] However, the measured cathodic scan of LDPT (Figure 2c) shows the onset of the cathodic wave at 0.20 V vs Li/Li^+. The decreased cathodic limit could be attributed to the presence of DCA^- anions in the LDPT electrolyte. In fact, DFT calculations on $Pyr_{14}DCA$[20] suggest that when an additional electron is introduced into the system, the spin-density around the terminal nitrogen atoms becomes anisotropic, making DCA^- more prone to electrophilic attacks on the opposite sides. However, the TCM^- anion structure is more symmetrical, leading to an isotropic distribution of the extra electron.[20] The cathodic peak observed below 0 V vs Li/Li^+ at about −0.1 V can be attributed to Li plating, while the exponential growth of the cathodic current (associated with the bulk decomposition of the electrolyte) appears at the same potential for both PT and LDPT.

Electrochemical Performance of Symmetrical Li/Li Cells. To demonstrate the compatibility between LDPT and Li, stripping/plating tests were performed at 20 °C in

symmetrical Li/LDPT/Li cells. The evolution of cell impedance during prolonged cycling was monitored by collecting the EIS spectra of the fresh cell (after the initial rest time at the OCV for 10 h) every 24 h during the initial 8 days of cycling and at the end of the experiment (after 1000 h of cycling). The voltage profile and the recorded impedance spectra are shown in Figure 3. The voltage profile (Figure 3a)

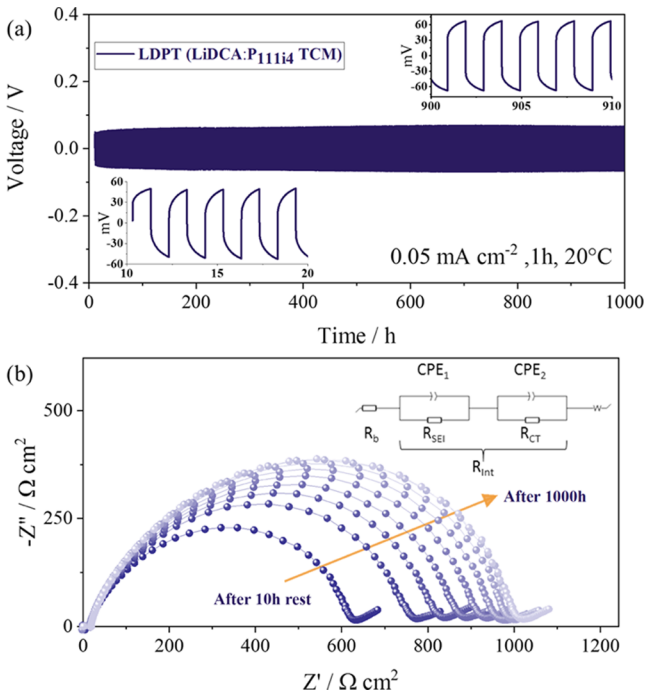

Figure 3. (a) Voltage profiles of symmetrical Li/LDPT/Li cells upon Li stripping/plating tests with a current of 0.05 mA cm ^{2} and a step length of 1 h. The insets show magnifications during five cycles after the rest time and 900 h. (b) Nyquist plots of the Li/LDPT/Li cell: specifically, after a 10 h rest period before testing, after every 12 cycles for 8 days, and after the final 400 cycles. The inset shows the equivalent circuit used to fit the impedance data.

shows an initial polarization of ±50 mV, gradually increasing to ±65 mV after prolonged cycling for 1000 h, displaying impressive cycling stability. The magnified voltage profiles are shown in the insets of Figure 3a highlight the stability of Li stripping and plating, evidenced by steady polarization profiles.

Figure 3b shows the Nyquist plots of the symmetrical cell together with the associated equivalent circuit used for fitting the spectra. The overall interfacial resistance (R_{Int}), corresponding to the broad feature encompassing the SEI resistance (R_{SEI}) and charge-transfer resistance (R_{CT}), results from summing up the two values for each spectrum. The parameters resulting from the EIS fitting are presented in Table S1. The interfacial resistance of the fresh cell (i.e., only upon contact with LDPT for 10 h at the OCV) was around 604 Ω cm^2. After 12 cycles (i.e., 24 h), it increased to ca. 733 Ω cm^2, suggesting the progressive accumulation of decomposition products on the Li surface, as a result of the spontaneous SEI formation. The impedance data acquired during the subsequent 96 cycles (i.e., the first 8 days of cycling) demonstrate that R_{Int} continues to evolve during cycling to ca. 985 Ω cm^2. Interestingly, however, upon the next 400 cycles (i.e., 800 h), it only increased to ca. 988 Ω cm^2. These impedance results, which are in agreement with the cell voltage evolution upon the galvanostatic stripping/plating test, indicate excellent long-term stability of the interphase formed between Li and LDPT. Stripping/plating tests at higher current densities were also performed, as shown in Figure S3. At 0.5 mA cm^{-2}, it was still possible to operate the cells for 20 cycles before the cell polarization increased beyond the cutoff limit of 1 V. When increasing the current density to 1 mA cm^{-2}, however, the cutoff was reached just after six cycles, suggesting the formation of a very resistive interface, which agrees with the EIS results previously discussed.

Moreover, the cycling performance of the LDPT electrolyte with LFP electrodes was investigated in three-electrode Li/LFP half-cells. As shown in Figure S4a, a gradual increase in capacity after the first cycle was observed, which can probably be assigned to improved electrode wetting upon cycling. Additionally, a capacity of 110 mAh g^{-1} and a Coulombic efficiency approaching 99% were achieved at the 10th cycle. This demonstrates the compatibility of such electrolyte with low-voltage cathodes.

Study of the Solid Electrolyte Interphase (SEI). To investigate the chemical composition of the SEI, the surface of the Li electrode after a single deposition step (i.e., 1 h at 0.05 mA cm^{-2}) was investigated by XPS. To gain insights into the depth distribution of the SEI species, the sample was subjected to Ar^+ ion sputtering too. High-resolution spectra were acquired after 5 and 10 min. Figure 4 shows the N 1s, C 1s, and P 2p core spectra of Li metal electrodes. Figures S5−S7 show the O 1s and Li 1s regions of the cycled and pristine electrodes.

Since the SEI is composed of both conducting and insulating compounds, surface charging is inevitable, resulting in the observation of different shifts for the signals of different compound types (differential charging effect).[49] For this reason, the peak assignment was done by the characteristic BE separations (ΔBEs) between the relevant core levels for specific species instead of using the common calibration method, i.e., assigning the −C−C− sp^3 peak at 284.8 eV as a reference.

As shown in Figure 4, despite washing with DMC, the outermost surface of the electrode showed LDPT complex ions (TCM^-, DCA^-, and P_{111i4}^+).[20,50,51] This is evident from the N 1s and P 2p spectra exhibiting features related to TCM^- (−C≡N, $\Delta BE_{(N\ 1s-C\ 1s)}$ = 112.56 ± 0.02 eV)[20,52] and DCA^- anions (C−N$^-$−C, $\Delta BE_{(N\ 1s-C\ 1s)}$ = 113.09 ± 0.07 eV),[20,51] as well as P_{111i4}^+ cations ($\Delta BE_{(C\ 1s-P\ 2p)}$ = 152.20 ± 0.07 eV).[53] The C 1s spectrum of the outermost surface (Figure 4, top row) also shows the signals associated with residual LDPT. These peaks, which correspond to species containing −C−C−/−C−H−, C−P$^+$, −C≡N, and −C−N− bonds, appear in the order of increasing BE.[20,51,53] Additionally, peaks attributed to species with the −O−C═O character (such as, e.g., lithium alkyl carbonate, $\Delta BE_{(O\ 1s-C\ 1s)}$ = 244.52 ± 0.08 eV)[59] and Li_2CO_3 ($\Delta BE_{(O\ 1s-C\ 1s)}$ = 241.80 ± 0.06 eV)[40] were also observed. Such characteristics may originate from the reaction of the residual Li salt and/or the electrode surface (not coated by the SEI) with DMC during the washing step.[20]

Upon 5 min of sputtering, the intensity of the LDPT-related peaks in the N 1s spectrum (i.e., −C≡N, $\Delta BE_{(N\ 1s-C\ 1s)}$ = 112.66 ± 0.02 eV and −C−N$^-$−C−, $\Delta BE_{(N\ 1s-C\ 1s)}$ = 112.62 ± 0.02 eV) decreased, indicating the decrease of residual LDPT. However, their presence might indicate the trapping of LDPT complex ions in the SEI. Additionally, three new peaks appeared, corresponding to the −N═C− double bond

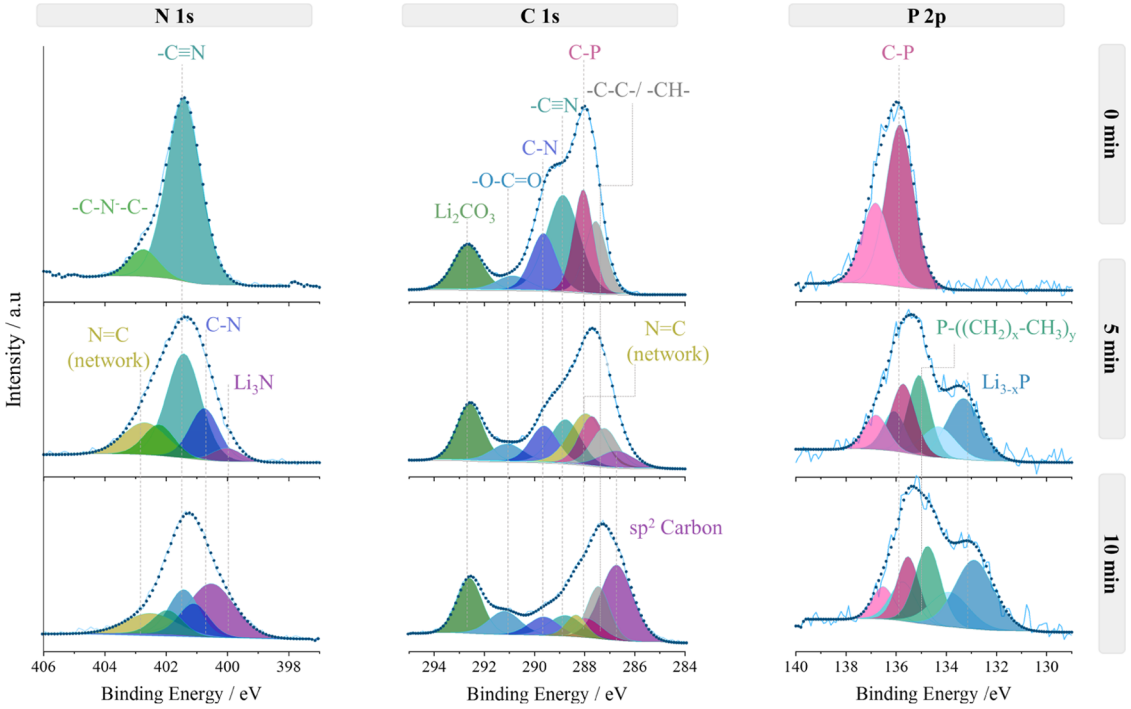

Figure 4. High-resolution N 1s, C 1s, and P 2p photoelectron spectra, before and after etching, of the Li-metal surface after the first lithium plating (current, 0.05 mA cm ^{2}; plating time, 1 h) in the LDPT electrolyte.

($\Delta BE_{(N\ 1s-C\ 1s)}$ = 114.75 ± 0.02 eV[54−57]) and −C−N− ($\Delta BE_{(N\ 1s-C\ 1s)}$ = 111.14 ± 0.02 eV[54−57]) in a polymeric network, as well as Li_3N ($\Delta BE_{(N\ 1s-Li\ 1s)}$ = 343.2 ± 0.02 eV[40,57]). These contributions are ascribed to the decomposition products of the anions. According to multiple previous studies on electrolytes composed of nitrile-base anions, the reductive polymerization of DCA and TCM anions results in the formation of the polymeric network, whereas the complete reduction forms Li_3N and graphitic carbon.[20,58−60] In line with these studies, a new, graphitic sp^2 carbon peak appears at about ∼0.8 eV lower than the −C−C−/−C−H− peak in the C 1s spectrum. Additionally, an increase in the intensity of the O═C−O and Li_2CO_3 peaks with sputtering time was observed, which could be attributed to the native SEI on the Li metal electrode. In fact, the lithium metal foil used is produced by extrusion and lamination in a 50:50 Ar/CO_2 atmosphere. After 10 min of sputtering in the N 1s spectrum, the two peaks related to TCM and DCA anions were still present (despite a significant decrease in the intensity), confirming that the LDPT complex ions were still embedded within the SEI structure.[36,61] Furthermore, the intensity of the peaks related to C and N atoms with single and double bonds in a polymeric network further decreased compared to the spectra obtained after 5 min of etching (in both N 1s and C 1s spectra). Exceptions are the Li_3N peak in the N 1s spectrum and the sp^2 and sp^3 carbon peaks in the C 1s region, both showing a significant increase. This may indicate the decomposition of both DCA^- and TCM^- anions due to the highly reducing environment in proximity of the Li metal surface.

Furthermore, the trend of the peaks associated with the LDPT complex ions upon sputtering reveals interesting information regarding the stability of the phosphonium cation. In comparison with the P 2p spectrum of the outermost surface, after sputtering, the peak broadened and shifted to lower BE values. After 5 min of sputtering, in addition to the P_{111i4}^+ peak, two new features at lower BE values were identified in the P 2p spectrum. Although the assignment of these features to specific degradation products requires further investigation, they can tentatively be assigned to neutral phosphorous surrounded by alkyl chains such as P−$((CH_2)_x$−$CH_3)_y$ (as it also occurs for the Pyr_{14}^+ cation[62]) and inorganic phosphides such as $Li_{3-x}P$,[63] which appear in the order of decreasing BE, respectively.

To the best of our knowledge, we are the first group ever to report the breakdown of this phosphonium cation when used in LIB/LMBs. In fact, Girard et al. did not detect any decomposition product of phosphonium in the SEI of the Li metal electrode after an extensive study on $P_{111i4}FSI$ by XPS, FTIR, and MAS-NMR.[38,61] However, a very recent study on triethyl(methyl)phosphonium bis(fluorosulfonyl)imide ($P_{1222}FSI$) for the Si anode reported by Araño et al. has shown that the cation can decompose when the salt concentration of the electrolyte is below a certain threshold (in that specific case, below 3.8 mol kg^{-1}).

On the basis of our XPS results, the SEI formed on the Li metal electrode in the presence of LDPT appears to be composed of two main layers: the outer layer that has a polymeric character, ensuring good mechanical flexibility, and the inner layer that is rich in inorganic compounds such as Li_3N and, probably, $Li_{3-x}P$, both of which are known to have high Li^+ ion conductivity.[64−66]

It is important to note that compared with our previous study on the single anion and mixed-anion systems combined with pyrrolidinium cations (i.e., LiDCA-Pyr_{14}DCA, LiTCM-Pyr_{14}TCM, and LiDCA-Pyr_{14}TCM), the SEI formed on the Li metal under the same conditions displayed very similar characteristics and composition.[20] Therefore, despite clear evidence of cation decomposition products, the SEI formation in cyano-based ILs is mainly anion-driven in both pyrrolidinium and phosphonium-based systems.

CONCLUSIONS

Herein, a new ionic liquid-based electrolyte containing a phosphonium cation and fluorine-free anions is proposed as a potential electrolyte for lithium metal batteries. The electrolyte LiDCA-P_{111i4}TCM (1:9 mol/mol ratio) exhibited high ionic conductivity (4.5 mS cm^{-1}), low viscosity (64.9 mPa s), and wide ESW (4 V) at room temperature. The electrolyte exhibited remarkable compatibility with Li metal, as evidenced by the prolonged Li stripping/plating test for over 800 cycles. The evolution of the Li/electrolyte interphase, investigated upon cycling *via* impedance spectroscopy, shows a relatively small increase after the first formation cycles. Finally, the SEI formed on the Li metal, characterized by XPS, appears to have a bilayer structure consisting of polymeric compounds and inorganic species in the outer and inner layers, respectively. According to the XPS data, the SEI is composed of reduction products of both anions (DCA and TCM) and the cation (P_{111i4}). In fact, despite prior studies reporting on the stability of the P_{111i4} cation against Li metal, the data revealed the decomposition of phosphonium cations into, possibly, ionic-conducting $Li_{3-x}P$. Although the decomposition products are evident, the exact reaction mechanism and breakdown pathways for this reduction require further investigation.

AUTHOR INFORMATION

Corresponding Authors

Alberto Varzi − *Helmholtz Institute Ulm (HIU), 89081 Ulm, Germany; Karlsruhe Institute of Technology (KIT), 76021 Karlsruhe, Germany;* orcid.org/0000-0001-5069-0589; Email: alberto.varzi@kit.edu

Stefano Passerini − *Helmholtz Institute Ulm (HIU), 89081 Ulm, Germany; Karlsruhe Institute of Technology (KIT), 76021 Karlsruhe, Germany;* orcid.org/0000-0002-6606-5304; Email: stefano.passerini@kit.edu

Authors

Niyousha Karimi − *Helmholtz Institute Ulm (HIU), 89081 Ulm, Germany; Karlsruhe Institute of Technology (KIT), 76021 Karlsruhe, Germany*

Maider Zarrabeitia − *Helmholtz Institute Ulm (HIU), 89081 Ulm, Germany; Karlsruhe Institute of Technology (KIT), 76021 Karlsruhe, Germany*

Milad Hosseini − *Helmholtz Institute Ulm (HIU), 89081 Ulm, Germany; Karlsruhe Institute of Technology (KIT), 76021 Karlsruhe, Germany*

Tugce Ates − *Helmholtz Institute Ulm (HIU), 89081 Ulm, Germany; Karlsruhe Institute of Technology (KIT), 76021 Karlsruhe, Germany*

Boyan Iliev − *IoLiTec-Ionic Liquids Technologies GmbH, 74076 Heilbronn, Germany*

Thomas J. S. Schubert − *IoLiTec-Ionic Liquids Technologies GmbH, 74076 Heilbronn, Germany*

Author Contributions

S.P. supervised the work and provided funding. A.V. supervised the work, designed the experiments, and discussed the data. N.K. designed and carried out experiments, analyzed, and discussed the data and wrote the paper. M.Z. performed the XPS experiments, analyzed, and discussed the data. M.H. carried out the electrochemical impedance data fitting. T.A. performed transference number measurements and Li/LFP cycling tests. B.I and T.J.S.S provided the ionic liquids. All authors reviewed the final version of the manuscript.

Notes

The authors declare no competing financial interest.

ACKNOWLEDGMENTS

This work was funded by the Bundesministerium für Bildung und Forschung (BMBF) with the project "NEILLSBAT" (Contract number 03XP0120A) within the M.Era-net framework. The authors also thank the Helmholtz Association for the financial support.

REFERENCES

(1) Horstmann, B.; Shi, J.; Amine, R.; Werres, M.; He, X.; Jia, H.; Hausen, F.; Cekic-Laskovic, I.; Wiemers-Meyer, S.; Lopez, J.; Galvez-Aranda, D.; Baakes, F.; Bresser, D.; Su, C.-C.; Xu, Y.; Xu, W.; Jakes, P.; Eichel, R.-A.; Figgemeier, E.; Krewer, U.; Seminario, J. M.; Balbuena, P. B.; Wang, C.; Passerini, S.; Shao-Horn, Y.; Winter, M.; Amine, K.; Kostecki, R.; Latz, A. Strategies towards Enabling Lithium Metal in Batteries: Interphases and Electrodes. *Energy Environ. Sci.* **2021**, *14*, 5289−5314.

(2) Schmuch, R.; Wagner, R.; Hörpel, G.; Placke, T.; Winter, M. Performance and Cost of Materials for Lithium-Based Rechargeable Automotive Batteries. *Nat. Energy* **2018**, *3*, 267−278.

(3) Peled, E. The Electrochemical Behavior of Alkali and Alkaline Earth Metals in Nonaqueous Battery Systems—The Solid Electrolyte Interphase Model. *J. Electrochem. Soc.* **1979**, *126*, 2047−2051.

(4) Wood, K. N.; Noked, M.; Dasgupta, N. P. Lithium Metal Anodes: Toward an Improved Understanding of Coupled Morphological, Electrochemical, and Mechanical Behavior. *ACS Energy Lett.* **2017**, *2*, 664−672.

(5) Kalhoff, J.; Eshetu, G. G.; Bresser, D.; Passerini, S. Safer Electrolytes for Lithium-Ion Batteries: State of the Art and Perspectives. *ChemSusChem* **2015**, *8*, 2154−2175.

(6) Wilken, S.; Treskow, M.; Scheers, J.; Johansson, P.; Jacobsson, P. Initial Stages of Thermal Decomposition of LiPF6-Based Lithium Ion Battery Electrolytes by Detailed Raman and NMR Spectroscopy. *RSC Adv.* **2013**, *3*, 16359−16364.

(7) Yang, H.; Zhuang, G. V.; Ross, P. N. Thermal Stability of LiPF6 Salt and Li-Ion Battery Electrolytes Containing LiPF6. *J. Power Sources* **2006**, *161*, 573−579.

(8) Zheng, L.; Zhang, H.; Cheng, P.; Ma, Q.; Liu, J.; Nie, J.; Feng, W.; Zhou, Z. Li[(FSO2)(n-C4F9SO2)N] versus LiPF6 for Graphite/LiCoO2 Lithium-Ion Cells at Both Room and Elevated Temperatures: A Comprehensive Understanding with Chemical, Electrochemical and XPS Analysis. *Electrochim. Acta* **2016**, *196*, 169−188.

(9) Wagner, R.; Korth, M.; Streipert, B.; Kasnatscheew, J.; Gallus, D. R.; Brox, S.; Amereller, M.; Cekic-Laskovic, I.; Winter, M. Impact of Selected LiPF6 Hydrolysis Products on the High Voltage Stability of

Lithium-Ion Battery Cells. *ACS Appl. Mater. Interfaces* **2016**, *8*, 30871−30878.
(10) Navarra, M. A. Ionic Liquids as Safe Electrolyte Components for Li-Metal and Li-Ion Batteries. *MRS Bull.* **2013**, *38*, 548−553.
(11) MacFarlane, D. R.; Forsyth, M.; Izgorodina, E. I.; Abbott, A. P.; Annat, G.; Fraser, K. On the Concept of Ionicity in Ionic Liquids. *Phys. Chem. Chem. Phys.* **2009**, *11*, 4962−4967.
(12) Macfarlane, D. R.; Tachikawa, N.; Forsyth, M.; Pringle, J. M.; Howlett, P. C.; Elliott, G. D.; Davis, J. H.; Watanabe, M.; Simon, P.; Angell, C. A. Energy Applications of Ionic Liquids. *Energy Environ. Sci.* **2014**, *7*, 232−250.
(13) Wang, X.; Salari, M.; Jiang, D. en.; Chapman Varela, J.; Anasori, B.; Wesolowski, D. J.; Dai, S.; Grinstaff, M. W.; Gogotsi, Y. Electrode Material−Ionic Liquid Coupling for Electrochemical Energy Storage. *Nat. Rev. Mater.* **2020**, *5*, 787−808.
(14) Armand, M.; Axmann, P.; Bresser, D.; Copley, M.; Edström, K.; Ekberg, C.; Guyomard, D.; Lestriez, B.; Novák, P.; Petranikova, M.; Porcher, W.; Trabesinger, S.; Wohlfahrt-Mehrens, M.; Zhang, H. Lithium-Ion Batteries − Current State of the Art and Anticipated Developments. *J. Power Sources* **2020**, *479*, No. 228708.
(15) Armand, M.; Tarascon, J.-M. Building Better Batteries. *Nature* **2008**, *451*, 652−657.
(16) Cano, Z. P.; Banham, D.; Ye, S.; Hintennach, A.; Lu, J.; Fowler, M.; Chen, Z. Batteries and Fuel Cells for Emerging Electric Vehicle Markets. *Nat. Energy* **2018**, *3*, 279−289.
(17) Larcher, D.; Tarascon, J. M. Towards Greener and More Sustainable Batteries for Electrical Energy Storage. *Nat. Chem.* **2015**, *7*, 19−29.
(18) Chu, S.; Majumdar, A. Opportunities and Challenges for a Sustainable Energy Future. *Nature* **2012**, *488*, 294−303.
(19) Dunn, B.; Kamath, H.; Tarascon, J. M. J.-M. Electrical Energy Storage for the Grid: A Battery of Choices. *Science* **2011**, *334*, 928−935.
(20) Karimi, N.; Zarrabeitia, M.; Mariani, A.; Gatti, D.; Varzi, A.; Passerini, S. Nonfluorinated Ionic Liquid Electrolytes for Lithium Metal Batteries: Ionic Conduction, Electrochemistry, and Interphase Formation. *Adv. Energy Mater.* **2021**, *11*, No. 2003521.
(21) Yoon, H.; Lane, G. H.; Shekibi, Y.; Howlett, P. C.; Forsyth, M.; Best, A. S.; MacFarlane, D. R. Lithium Electrochemistry and Cycling Behaviour of Ionic Liquids Using Cyano Based Anions. *Energy Environ. Sci.* **2013**, *6*, 979.
(22) MacFarlane, D. R.; Golding, J.; Forsyth, S.; Forsyth, M.; Deacon, G. B. Low Viscosity Ionic Liquids Based on Organic Salts of the Dicyanamide Anion. *Chem. Commun.* **2001**, *16*, 1430−1431.
(23) Chaban, V. V. The Tricyanomethanide Anion Favors Low Viscosity of the Pure Ionic Liquid and Its Aqueous Mixtures. *Phys. Chem. Chem. Phys.* **2015**, *17*, 31839−31849.
(24) MacFarlane, D. R.; Forsyth, S. A.; Golding, J.; Deacon, G. B. Ionic Liquids Based on Imidazolium and Pyrrolidinium Salts of the Tricyanomethanide Anion. *Green Chem.* **2002**, *4*, 444−448.
(25) Shen, S.; Fang, S.; Qu, L.; Luo, D.; Yang, L.; Hirano, S. I. Low-Viscosity Ether-Functionalized Pyrazolium Ionic Liquids Based on Dicyanamide Anions: Properties and Application as Electrolytes for Lithium Metal Batteries. *RSC Adv.* **2015**, *5*, 93888−93899.
(26) Park, J. W.; Ueno, K.; Tachikawa, N.; Dokko, K.; Watanabe, M. Ionic Liquid Electrolytes for Lithium-Sulfur Batteries. *J. Phys. Chem. C* **2013**, *117*, 20531−20541.
(27) Appetecchi, G. B.; Montanino, M.; Passerini, S. Ionic Liquid-Based Electrolytes for High Energy, Safer Lithium Batteries. *ACS Symp. Ser.* **2012**, *1117*, 67−128.
(28) Basile, A.; Bhatt, A. I.; O'Mullane, A. P. Stabilizing Lithium Metal Using Ionic Liquids for Long-Lived Batteries. *Nat. Commun.* **2016**, *7*, No. 11794.
(29) Moreno, M.; Simonetti, E.; Appetecchi, G. B.; Carewska, M.; Montanino, M.; Kim, G.-T.; Loeffler, N.; Passerini, S. Ionic Liquid Electrolytes for Safer Lithium Batteries. *J. Electrochem. Soc.* **2017**, *164*, A6026−A6031.
(30) Howlett, P. C.; MacFarlane, D. R.; Hollenkamp, A. F. High Lithium Metal Cycling Efficiency in a Room-Temperature Ionic Liquid. *Electrochem. Solid-State Lett.* **2004**, *7*, A97−A101.
(31) Grande, L.; von Zamory, J.; Koch, S. L.; Kalhoff, J.; Paillard, E.; Passerini, S. Homogeneous Lithium Electrodeposition with Pyrrolidinium-Based Ionic Liquid Electrolytes. *ACS Appl. Mater. Interfaces* **2015**, *7*, 5950−5958.
(32) Galiński, M.; Lewandowski, A.; Stepniak, I. Ionic Liquids as Electrolytes. *Electrochim. Acta* **2006**, *51*, 5567−5580.
(33) Tsunashima, K.; Kodama, S.; Sugiya, M.; Kunugi, Y. Physical and Electrochemical Properties of Room-Temperature Dicyanamide Ionic Liquids Based on Quaternary Phosphonium Cations. *Electrochim. Acta* **2010**, *56*, 762−766.
(34) Girard, G. M. A.; Hilder, M.; Zhu, H.; Nucciarone, D.; Whitbread, K.; Zavorine, S.; Moser, M.; Forsyth, M.; MacFarlane, D. R.; Howlett, P. C. Electrochemical and Physicochemical Properties of Small Phosphonium Cation Ionic Liquid Electrolytes with High Lithium Salt Content. *Phys. Chem. Chem. Phys.* **2015**, *17*, 8706−8713.
(35) Wu, F.; Schür, A. R.; Kim, G.-T.; Dong, X.; Kuenzel, M.; Diemant, T.; D'Orsi, G.; Simonetti, E.; De Francesco, M.; Bellusci, M.; Appetecchi, G. B.; Passerini, S. A Novel Phosphonium Ionic Liquid Electrolyte Enabling High-Voltage and High-Energy Positive Electrode Materials in Lithium-Metal Batteries. *Energy Storage Mater.* **2021**, *42*, 826−835.
(36) Girard, G. M. A.; Hilder, M.; Nucciarone, D.; Whitbread, K.; Zavorine, S.; Moser, M.; Forsyth, M.; MacFarlane, D. R.; Howlett, P. C. Role of Li Concentration and the SEI Layer in Enabling High Performance Li Metal Electrodes Using a Phosphonium Bis-(Fluorosulfonyl)Imide Ionic Liquid. *J. Phys. Chem. C* **2017**, *121*, 21087−21095.
(37) Hilder, M.; Girard, G. M. A.; Whitbread, K.; Zavorine, S.; Moser, M.; Nucciarone, D.; Forsyth, M.; MacFarlane, D. R.; Howlett, P. C. Physicochemical Characterization of a New Family of Small Alkyl Phosphonium Imide Ionic Liquids. *Electrochim. Acta* **2016**, *202*, 100−109.
(38) Girard, G. M. A.; Hilder, M.; Dupre, N.; Guyomard, D.; Nucciarone, D.; Whitbread, K.; Zavorine, S.; Moser, M.; Forsyth, M.; MacFarlane, D. R.; Howlett, P. C. Spectroscopic Characterization of the SEI Layer Formed on Lithium Metal Electrodes in Phosphonium Bis(Fluorosulfonyl)Imide Ionic Liquid Electrolytes. *ACS Appl. Mater. Interfaces* **2018**, *10*, 6719−6729.
(39) Elgrishi, N.; Rountree, K. J.; McCarthy, B. D.; Rountree, E. S.; Eisenhart, T. T.; Dempsey, J. L. A Practical Beginner's Guide to Cyclic Voltammetry. *J. Chem. Educ.* **2018**, *95*, 197−206.
(40) Wood, K. N.; Teeter, G. XPS on Li-Battery-Related Compounds: Analysis of Inorganic SEI Phases and a Methodology for Charge Correction. *ACS Appl. Energy Mater.* **2018**, *1*, 4493−4504.
(41) Ferraresi, G.; Czornomaz, L.; Villevieille, C.; Novák, P.; El Kazzi, M. Elucidating the Surface Reactions of an Amorphous Si Thin Film as a Model Electrode for Li-Ion Batteries. *ACS Appl. Mater. Interfaces* **2016**, *8*, 29791−29798.
(42) Tsunashima, K.; Yonekawa, F.; Kikuchi, M.; Sugiya, M. Effect of Quaternary Phosphonium Salts in Organic Electrolyte for Lithium Secondary Batteries. *Electrochemistry* **2011**, *79*, 453−457.
(43) Markevich, E.; Baranchugov, V.; Salitra, G.; Aurbach, D.; Schmidt, M. A. Behavior of Graphite Electrodes in Solutions Based on Ionic Liquids in In Situ Raman Studies. *J. Electrochem. Soc.* **2008**, *155*, A132.
(44) Borgel, V.; Markevich, E.; Aurbach, D.; Semrau, G.; Schmidt, M. On the Application of Ionic Liquids for Rechargeable Li Batteries: High Voltage Systems. *J. Power Sources* **2009**, *189*, 331−336.
(45) Matsumoto, H.; Kageyama, H.; Miyazaki, Y. Effect of Ionic Additives on the Limiting Cathodic Potential of EMI-Based Room Temperature Ionic Liquids. *Electrochemistry* **2003**, *71*, 1058−1060.
(46) Shin, J.-H.; Henderson, W. A.; Passerini, S. PEO-Based Polymer Electrolytes with Ionic Liquids and Their Use in Lithium Metal-Polymer Electrolyte Batteries. *J. Electrochem. Soc.* **2005**, *152*, A978.

(47) Hoffknecht, J. P.; Drews, M.; He, X.; Paillard, E. Investigation of the N-Butyl-N-Methyl Pyrrolidinium Trifluoromethanesulfonyl-N-Cyanoamide (PYR14TFSAM) Ionic Liquid as Electrolyte for Li-Ion Battery. *Electrochim. Acta* **2017**, *250*, 25−34.
(48) Liu, C.; Ma, X.; Xu, F.; Zheng, L.; Zhang, H.; Feng, W.; Huang, X.; Armand, M.; Nie, J.; Chen, H.; Zhou, Z. Ionic Liquid Electrolyte of Lithium Bis(Fluorosulfonyl)Imide/N-Methyl-N-Propylpiperidinium Bis(Fluorosulfonyl)Imide for Li/Natural Graphite Cells: Effect of Concentration of Lithium Salt on the Physicochemical and Electrochemical Properties. *Electrochim. Acta* **2014**, *149*, 370−385.
(49) Philippe, B.; Dedryvère, R.; Allouche, J.; Lindgren, F.; Gorgoi, M.; Rensmo, H.; Gonbeau, D.; Edström, K. Nanosilicon Electrodes for Lithium-Ion Batteries: Interfacial Mechanisms Studied by Hard and Soft X-Ray Photoelectron Spectroscopy. *Chem. Mater.* **2012**, *24*, 1107−1115.
(50) Sun, J.; O'Dell, L. A.; Armand, M.; Howlett, P. C.; Forsyth, M. Anion-Derived Solid-Electrolyte Interphase Enables Long Life Na-Ion Batteries Using Superconcentrated Ionic Liquid Electrolytes. *ACS Energy Lett.* **2021**, *6*, 2481−2490.
(51) Howlett, P. C.; Brack, N.; Hollenkamp, A. F.; Forsyth, M.; MacFarlane, D. R. Characterization of the Lithium Surface in N -Methyl- N -Alkylpyrrolidinium Bis(Trifluoromethanesulfonyl)Amide Room-Temperature Ionic Liquid Electrolytes. *J. Electrochem. Soc.* **2006**, *153*, A595.
(52) Rossi, F.; Andre, B.; van Veen, A.; Miinarends, P. E.; Schut, H.; Labohm, F.; Dunlop, H.; Delnlancke, M. P.; Hubbard, K. Physical Properties of A-C: N Films Produced by Ion Beam Assisted Deposition. *J. Mater. Res.* **1994**, *9*, 2440−2449.
(53) Blundell, R. K.; Licence, P. Quaternary Ammonium and Phosphonium Based Ionic Liquids: A Comparison of Common Anions. *Phys. Chem. Chem. Phys.* **2014**, *16*, 15278−15288.
(54) Bhattacharyya, S.; Hong, J.; Turban, G. Determination of the Structure of Amorphous Nitrogenated Carbon Films by Combined Raman and X-Ray Photoemission Spectroscopy. *J. Appl. Phys.* **1998**, *83*, 3917−3919.
(55) Dementjev, A. P.; De Graaf, A.; Van de Sanden, M. C. M.; Maslakov, K. I.; Naumkin, A. V.; Serov, A. A. X-Ray Photoelectron Spectroscopy Reference Data for Identification of the C3N4 Phase in Carbon-Nitrogen Films. *Diamond Relat. Mater.* **2000**, *9*, 1904−1907.
(56) Bhattacharyya, S.; Cardinaud, C.; Turban, G. Spectroscopic Determination of the Structure of Amorphous Nitrogenated Carbon Films. *J. Appl. Phys.* **1998**, *83*, 4491−4500.
(57) Buchner, F.; Bozorgchenani, M.; Uhl, B.; Farkhondeh, H.; Bansmann, J.; Behm, R. J. Reactive Interaction of (Sub-)Monolayers and Multilayers of the Ionic Liquid 1-Butyl-1-Methylpyrrolidinium Bis(Trifluoro-Methylsulfonyl)Imide with Coadsorbed Lithium on Cu(111). *J. Phys. Chem. C* **2015**, *119*, 16649−16659.
(58) Paraknowitsch, J. P.; Zhang, J.; Su, D.; Thomas, A.; Antonietti, M. Ionic Liquids as Precursors for Nitrogen-Doped Graphitic Carbon. *Adv. Mater.* **2010**, *22*, 87−92.
(59) Wooster, T. J.; Johanson, K. M.; Fraser, K. J.; MacFarlane, D. R.; Scott, J. L. Thermal Degradation of Cyano Containing Ionic Liquids. *Green Chem.* **2006**, *8*, 691−696.
(60) Zhang, H.; Judez, X.; Santiago, A.; Martinez-Ibañez, M.; Muñoz-Márquez, M. Á.; Carrasco, J.; Li, C.; Eshetu, G. G.; Armand, M. Fluorine-Free Noble Salt Anion for High-Performance All-Solid-State Lithium−Sulfur Batteries. *Adv. Energy Mater.* **2019**, *9*, No. 1900763.
(61) Araño, K.; Mazouzi, D.; Kerr, R.; Lestriez, B.; Le Bideau, J.; Howlett, P. C.; Dupré, N.; Forsyth, M.; Guyomard, D. Editors' Choice—Understanding the Superior Cycling Performance of Si Anode in Highly Concentrated Phosphonium-Based Ionic Liquid Electrolyte. *J. Electrochem. Soc.* **2020**, *167*, No. 120520.
(62) Kroon, M. C.; Buijs, W.; Peters, C. J.; Witkamp, G. J. Decomposition of Ionic Liquids in Electrochemical Processing. *Green Chem.* **2006**, *8*, 241−245.
(63) Wood, K. N.; Steirer, K. X.; Hafner, S. E.; Ban, C.; Santhanagopalan, S.; Lee, S. H.; Teeter, G. Operando X-Ray Photoelectron Spectroscopy of Solid Electrolyte Interphase Formation and Evolution in Li2S-P2S5 Solid-State Electrolytes. *Nat. Commun.* **2018**, *9*, No. 2490.
(64) Alpen, U. V.; Rabenau, A.; Talat, G. H. Ionic Conductivity in Li3N Single Crystals. *Appl. Phys. Lett.* **1977**, *30*, 621−623.
(65) Wang, A.; Kadam, S.; Li, H.; Shi, S.; Qi, Y. Review on Modeling of the Anode Solid Electrolyte Interphase (SEI) for Lithium-Ion Batteries. *npj Comput. Mater.* **2018**, *4*, No. 15.
(66) Qi, S.; He, J.; Liu, J.; Wang, H.; Wu, M.; Li, F.; Wu, D.; Li, X.; Ma, J. Phosphonium Bromides Regulating Solid Electrolyte Interphase Components and Optimizing Solvation Sheath Structure for Suppressing Lithium Dendrite Growth. *Adv. Funct. Mater.* **2021**, *31*, No. 2009013.
(67) Varzi, A.; Bresser, D.; von Zamory, J.; Müller, F.; Passerini, S. ZnFe 2 O 4 -C/LiFePO 4 -CNT: A Novel High-Power Lithium-Ion Battery with Excellent Cycling Performance. *Adv. Energy Mater.* **2014**, *4*, No. 1400054.